J. Fluid Mech. (1971), *vol.* 48, *part* 3, *pp.* 477–505
Printed in Great Britain

The determination of the rate of dissipation in turbulent pipe flow

By C. J. LAWN

Central Electricity Generating Board,
Berkeley Nuclear Laboratories,
Berkeley, Gloucestershire

(Received 12 May 1970)

Measurements of turbulence energy diffusion and the spectral distributions of stress components in the core of turbulent pipe flow are presented. The results tend to confirm the proposal of Bradshaw (1967*a*, *b*) that an inertial subrange in the spectra can exist at quite modest laboratory Reynolds numbers. They also illuminate the inconsistencies in Laufer's (1954) measurements of dissipation and suggest that the fitting of a $-\frac{5}{3}$ power law to the spectra may well provide the most accurate method of determining dissipation for $Re \gtrsim 10^5$.

1. Introduction

Studies of the turbulence energy processes in shear flows have all suffered from uncertainty in determining the rate of turbulent dissipation into heat. As shown by Hinze (1959), this is given precisely by

$$\epsilon = \nu \sum_{i,j} \overline{\left(\frac{\partial u_i}{\partial x_j} + \frac{\partial u_j}{\partial x_i}\right) \frac{\partial u_i}{\partial x_j}}, \tag{1.1}$$

(where u_i is the component of the fluctuating velocity in the x_i direction) but the approximation of homogeneity in the small-scale motions, which clearly contribute most significantly to the dissipation, reduces this expression to the more convenient form

$$\epsilon = \nu \sum_{i,j} \overline{\left(\frac{\partial u_i}{\partial x_j}\right)^2}. \tag{1.2}$$

The 'classical' approach to determining ϵ is to measure some (up to five) of the nine contributions to this sum, and to assume that isotropic relations may be used to derive the remainder. This is the method of Laufer (1954) for pipe flow, and Klebanoff (1955) for a boundary layer, both investigations being conducted with the same equipment.

As Laufer himself indicated, his results contained several inconsistencies: these will be discussed further in the next section. Moreover, the method is laborious and time-consuming and its accuracy depends critically upon the high-frequency response of the hot-wire equipment and the validity of the isotropic assumptions. Unfortunately accuracy is often required in these studies because of the requirement to identify the small differences in the rates of production and dissipation of

turbulence, which indicate that the fluid layer is not in a state of equilibrium. There is thus a strong incentive to devise a method for inferring ϵ without recourse to measurements of the velocity derivatives.

Bradshaw (1967*a*, *b*) has proposed a suitable method in which the Kolmogoroff (1941) hypothesis of an inertial subrange is assumed to apply to a relatively easily measured region of the one-dimensional spectrum function. Stringent conditions which are seldom fulfilled in laboratory flows for the existence of the inertial subrange, have been propounded by several workers, such as Stewart & Townsend (1951) and Batchelor (1956), but Bradshaw has suggested that sufficient conditions are in fact quite frequently fulfilled.

The Kolmogoroff hypothesis of universal equilibrium, as discussed by Batchelor (1956), is based upon the statistical independence of the components of fluctuating velocity at high wave-number, and hence the existence of 'local' isotropy. For these high wave-number dissipating motions to be in equilibrium, they must be independent of the wave-numbers associated with the conversion of energy from the mean flow. (Since this 'production' of turbulence is by the working of the Reynolds stresses against the mean strain field, these wave-numbers are anisotropic by definition.) Complete independence requires that the two ranges do not overlap at all, but the practical implication of the equilibrium hypothesis, that the equilibrium range of wave-numbers is uniquely determined statistically by the parameters ϵ and ν, may well hold to a good approximation when there is some overlap. The only necessary condition for the spectrum of a velocity component to have an equilibrium range appears to be that the rates of production, diffusion (from other layers of the flow), and transfer from other components, be small compared with the rates of dissipation and of inertial transfer through the spectrum in that range. Complete isotropy is therefore not required but the condition that the transfer from one component to another be relatively small suggests that the normal stresses due to these components will be approximately equal in the wave-number range.

This condition, termed 'second-class local isotropy' by Bradshaw, does not preclude the existence of shear, and in fact includes an inherent anisotropy by giving special emphasis to the direction of flow and any two directions at right angles. The reason for this could be that in boundary-layer flows all turbulence energy is initially produced in the component in the flow direction and then distributed among the other components through the pressure fluctuations. The distribution is probably most rapid in the perpendicular directions, tending to equalize these components before isotropy extends to the whole stress field.

Furthermore, the hypothesis of a subrange at the low wave-number end of the equilibrium range, in which there is independence of viscosity also, may only necessitate that the rate of dissipation be small in that subrange compared with the remaining process, that of inertial transfer through the spectrum. Since the spectral function can then depend only on ϵ, the rate of inertial transfer as well as dissipation, dimensional analysis shows that it must have the form

$$E(k) = \alpha k^{-\frac{5}{3}} \epsilon^{\frac{2}{3}} \tag{1.3}$$

in this 'inertial subrange'. If indeed this equation holds when production, dif-

fusion and dissipation are small, but appreciable, fractions of the total energy exchange, then it does provide a comparatively easy method of measuring ϵ in laboratory shear flows. Only recourse to experiment will decide whether this is in fact a sufficient condition.

In an attempt to quantify the condition, Bradshaw (1967*a*) examined results for grid turbulence and boundary layers and proposed

$$10/l < k < 0{\cdot}1/\eta, \tag{1.4}$$

where l is the length-scale of the energy-containing eddies, defined as

$$l = (2\overline{u^2}/3\epsilon)^{\frac{3}{2}},$$

and η is the Kolmogoroff length-scale for the equilibrium range,

$$\eta = \left(\frac{\nu^3}{\epsilon}\right)^{\frac{1}{4}}.$$

In practice, the one-dimensional spectrum only is measured and the condition was found to be

$$10/l < k_1 < 0{\cdot}07/\eta, \tag{1.5}$$

so that if an inertial subrange is to exist,

$$l/\eta > 10/0{\cdot}07. \tag{1.6}$$

When this condition was satisfied, Bradshaw found

$$E(k_1) = K\epsilon^{\frac{2}{3}}k_1^{-\frac{5}{3}}, \tag{1.7}$$

where $K \simeq 0{\cdot}55$ in the outer layers of shear flows, and $\simeq 0{\cdot}51$ in the inner layers.

As will be shown in the next section, the condition (1.6) is fulfilled in pipe flow at quite modest Reynolds numbers. It was therefore disappointing to discover that Laufer's results are not compatible with the existence of any kind of local isotropy, but Bradshaw concluded that this was not sufficient evidence for his proposal to be refuted.

This view is substantiated by the present work. Measurements of the production and kinetic energy diffusion terms in the turbulence energy equation have been made by the author for the flow of air through a pipe. These are described in §3. By estimating the contribution of pressure diffusion, the rate of dissipation in the core region has been deduced as the closing term in the equation. This is compared in §4 with dissipation estimated by the 'classical' method from one-dimensional power spectral density and spatial correlation measurements. At $Re = 9 \times 10^4$, a high degree of isotropy was found in the dissipating motions and this is in accord with the finding of §5, that the rate of dissipation may be accurately determined by the Kolmogoroff–Bradshaw hypothesis.

2. Dissipation in pipe flow

2.1. *Similarity considerations*

The turbulence energy equation for the fully-developed steady flow of fluid in a pipe of radius a may be written in cylindrical co-ordinates

$$-\overline{uv}\frac{dU}{dr} - \frac{1}{r}\frac{d}{dr}\left\{r\left(\frac{\overline{vq^2}}{2} + \frac{\overline{vp}}{\rho}\right)\right\} = \nu\overline{\sum_{i,j}\left(\frac{\partial u_i}{\partial x_j}\right)^2} = \epsilon, \tag{2.1}$$

where $q^2 = \overline{u^2+v^2+w^2}$, and the small type denotes fluctuating quantities. Certain viscous terms have been neglected on the grounds that they are

$$O(\nu u_\tau^2/a^2)$$

(whereas the remaining two on the left-hand side are $O(u_\tau^3/a)$) and are thus negligible at turbulent Reynolds numbers in the core region of the flow. This core region embraces those parts of the flow at which the velocity defect and the fluctuating velocities, when normalized by the wall friction velocity, are invariant with respect to Reynolds number. It is expected that this Reynolds number similarity extends to the triple velocity products also, so that the production and diffusion terms are in fact proportional to u_τ^3/a as well as being of that order. In this case, the dissipation rate must have the same proportionality, and if the microscales are defined in the usual way,

$$\begin{bmatrix} \overline{\left(\frac{\partial u}{\partial x}\right)^2} & \overline{\left(\frac{\partial v}{\partial x}\right)^2} & \overline{\left(\frac{\partial w}{\partial x}\right)^2} \\ \overline{\left(\frac{\partial u}{\partial r}\right)^2} & \overline{\left(\frac{\partial v}{\partial r}\right)^2} & \overline{\left(\frac{\partial w}{\partial r}\right)^2} \\ \frac{1}{r^2}\overline{\left(\frac{\partial u}{\partial \phi}\right)^2} & \frac{1}{r^2}\overline{\left(\frac{\partial v}{\partial \phi}\right)^2} & \frac{1}{r^2}\overline{\left(\frac{\partial w}{\partial \phi}\right)^2} \end{bmatrix} \equiv \begin{bmatrix} \frac{\overline{u^2}}{\lambda_{xu}^2} & \frac{2\overline{v^2}}{\lambda_{xv}^2} & \frac{2\overline{w^2}}{\lambda_{xw}^2} \\ \frac{2\overline{u^2}}{\lambda_{ru}^2} & \frac{\overline{v^2}}{\lambda_{rv}^2} & \frac{2\overline{w^2}}{\lambda_{rw}^2} \\ \frac{2\overline{u^2}}{\lambda_{\varphi u}^2} & \frac{2\overline{v^2}}{\lambda_{\phi v}^2} & \frac{\overline{w^2}}{\lambda_{\phi w}^2} \end{bmatrix}, \tag{2.2}$$

their Reynolds number dependence is established by the above argument, provided the structure of the dissipating motions is also preserved. For

$$\frac{a\epsilon}{u_\tau^3} = \frac{a\nu}{u_\tau^3}\sum_{i,j}\overline{\left(\frac{\partial u_i}{\partial x_j}\right)^2} = \frac{1}{a^+}\sum_{i,j}\left(\frac{\overline{u_j^2}}{u_\tau^2}\right)\Big/\left(\frac{\lambda_{x_i u_j}^2}{a^2}\right)2^{1-\delta_{ij}} \tag{2.3}$$

must be independent of Reynolds number, so

$$\lambda_{x_i u_j}/a \propto (a^+)^{-\frac{1}{2}}, \tag{2.4}$$

where the superscript $^+$ denotes non-dimensionalization by ν and u_τ. This proportionality provides a test for the accuracy of measurements of microscales. Total isotropy is indicated if the λ's are all equal as well as the $\overline{u_i^2}$'s, so in that case

$$\epsilon = 15\nu\frac{\overline{u^2}}{\lambda_{xu}^2} = 15\nu\overline{\left(\frac{\partial u}{\partial x}\right)^2}. \tag{2.5}$$

(See Hinze 1959.) If only the small-scale motion is isotropic then (2.5) still holds, although $\overline{u^2} \neq \overline{v^2} \neq \overline{w^2}$ and the λ's are not all equal.

2.2. *Laufer's measurements of dissipation*

With the above similarity consideration in mind, Laufer made measurements at two widely separated Reynolds numbers and corrected errors in one set by reference to the other. It should be noted that his constant-current hot-wire equipment did not include linearizers, and this must have complicated the measurements. Indeed those of diffusion, involving triple correlations, are likely to be seriously in error, due to distortion, and this is substantiated by large discrepancies in the results for the two Reynolds numbers.

The microscales were measured in two ways, λ_{xu}, λ_{xv} and λ_{xw} by electronic differentiation of the hot-wire signals and the assumption that Taylor's hypothesis holds, and λ_{ru} and $\lambda_{\phi u}$ by physically separating two wires and measuring the correlation coefficient between their signals. The total value for dissipation in the pipe at $Re = 4{\cdot}0 \times 10^4$, obtained by assuming the isotropic relations between derivatives

$$2\overline{\left(\frac{\partial v}{\partial r}\right)^2} = \overline{\left(\frac{\partial w}{\partial r}\right)^2} = \overline{\left(\frac{\partial u}{\partial r}\right)^2} \tag{2.6}$$

and

$$\frac{1}{r^2}\overline{\left(\frac{\partial v}{\partial \phi}\right)^2} = \frac{2}{r^2}\overline{\left(\frac{\partial w}{\partial \phi}\right)^2} = \frac{1}{r^2}\overline{\left(\frac{\partial u}{\partial \phi}\right)^2}$$

came to within 10 % of the total production. Of the other isotropic relations,

$$2\overline{\left(\frac{\partial u}{\partial x}\right)^2} = \overline{\left(\frac{\partial v}{\partial x}\right)^2} = \overline{\left(\frac{\partial w}{\partial x}\right)^2} \tag{2.7}$$

held approximately but

$$\overline{\left(\frac{\partial u}{\partial x}\right)^2} = \overline{\left(\frac{\partial v}{\partial r}\right)^2} = \frac{1}{r^2}\overline{\left(\frac{\partial w}{\partial \phi}\right)^2} \tag{2.8}$$

was apparently so far in error that use of equation (2.5) would have made the total ϵ for the pipe too small by a factor of 2·5. At $Re = 4{\cdot}3 \times 10^5$ the values of dissipation inferred from production and diffusion were everywhere 100 % greater than those estimated from the microscale measurements, and this is reflected in the failure of the microscales to vary according to equation (2.4).

Assuming the validity of the triple correlations at the higher Reynolds number, and the microscale measurements at the lower, Laufer showed, by taking it to be the closing term in (2.1), that the diffusion of pressure energy is small in the core region, compared with the diffusion of kinetic energy. As both the kinetic energy diffusion and dissipation rates may well have been inaccurately determined, this evidence is slim: neither should evidence regarding lack of isotropy in the small-scale motion be regarded as conclusive.

2.3. *The existence of an inertial subrange*

The approximate condition (1.6) may be translated into easily appreciable terms by substitution in terms of λ_{xu} and use of (2.5). (The definition of l for homogeneous grid-turbulence is retained for shear flows, although $\overline{u^2} \neq \frac{1}{3}q^2$, for convenience.) The condition becomes

$$Re_\lambda \gtrsim 140, \tag{2.9}$$

where

$$Re_\lambda \equiv \tilde{u}\lambda_{xu}/\nu,$$

and since Laufer's higher Reynolds number results were all at $Re_\lambda > 200$, an inertial subrange in his spectra is expected on the evidence of the flows examined by Bradshaw. Laufer did indeed find an appreciable range ($10 < ak_1 < 200$) of his spectrum which varied as $k_1^{-\frac{5}{3}}$, at the higher Reynolds number, but calculation of the dissipation according to (1.7) for a radial position of $r/a = 0{\cdot}72$ gives a value about $\frac{1}{2}$ of the measured, and only $\frac{1}{4}$ of that deduced from the more reliable low

Reynolds number results. The measured spectra of the components did not obey the isotropic relation

$$2E_v^2(k_1) = E_u^2(k_1) - k_1 \frac{\partial E_u^2(k_1)}{\partial k_1} \tag{2.10}$$

in this range either.

It is extremely unlikely that the differences between boundary-layer and pipe flows can cause a breakdown of the inertial subrange: there is thus basic disagreement between the data of Laufer and Bradshaw. A programme of measurements to check Laufer's work is described in the next section.

Some evidence in favour of Bradshaw's conclusions has already been provided by Comte-Bellot's (1965) study of channel flow. She found $K = 0{\cdot}51$, at least when $Re_\lambda > 300$.

3. Basic experimental results

3.1. *Equipment*

Details of the experimental arrangement are given in Lawn (1970): the salient features are as follows. Air was blown through a honed channel, 14·43 cm in diameter, and 60 diameters in length. Measurements were made in a plane one diameter below the outlet to atmosphere. The surface of the pipe at the inlet was roughened to promote flow development.

Mean velocity measurements were made with a total head tube and this was also used to calibrate the mass flow meter and the three hot-wire probes. Two of these were DISA standard single and X-wire probes: the third was specially made to allow accurate separation of two parallel wires. Pressures from 25 wall-tappings, equally spaced along the channel, and the mass flow rate from the calibrated device on the fan inlet, were used to determine the friction factor initially: in some of the later runs, the mass flow rate alone was recorded and the wall shear stress deduced from the friction factor curve.

The anemometers were DISA constant-temperature devices with linearization. Details of the processing system and operating techniques are to be found in Lawn (1969, 1970). Stability of the X wires was achieved at a gain setting which gave a flat frequency response to 3 kHz at an air velocity of 10 m/sec, with the -3dB point at 16 kHz. Somewhat poorer response was accepted for the single wire probes. Signals were squared when necessary by a Fenlow MX 101 analogue multiplier, and a Leevers-rich E44M FM tape recorder was used in the analysis. First, the tape recorder allowed frequency transformation of signals by factors of up to 32, so that steady r.m.s. readings of low-frequency components could be obtained; and secondly it made possible the measurement of the real component of cross-spectral density, using the same wave analyser, a Muirhead K-124-A, on both channels. Considerable care was taken to ensure that the frequency response of the modulator and demodulator circuits at the selected tape speeds were adequate for the task in hand. Correlation measurements were performed on a DISA 55D70 analogue correlator.

In X-wire measurements, the sensitivities of the two wires were carefully matched and the mean measured from the calibration plots to an estimated $\pm 1\%$.

To improve upon the accuracy of the correlation between the two velocity components, which depends critically upon the accuracy of matching, the mean result of two traverses (the second with the relative wire positions reversed) was taken in each run.

The response of a wire to yaw was assumed to have the form

$$U_{\text{eff}} = U(\cos^2\beta + k_\beta^2 \sin^2\beta)^{\frac{1}{2}}, \tag{3.1}$$

where β is the angle of the wire-normal to the velocity vector. This was checked with one of the probes in a controlled yaw experiment which gave $k_\beta = 0{\cdot}23$ in the velocity range of present interest, 10 m/sec $< U <$ 45 m/sec. No corrections for wall interference, turbulence intensity, or wire-length effects were made (see § 3.5).

3.2. *Preliminary results*

Velocity traverses in four quadrants of the pipe showed that a mean profile described the flow distribution to within $\pm 0{\cdot}5$ %. The friction factor results agreed with the correlations

$$f = 0{\cdot}079\, Re^{-0.25}, \quad 3 \times 10^4 < Re < 10^5 \tag{3.2}$$

and

$$f = 0{\cdot}046\, Re^{-0.20}, \quad 2 \times 10^5 < Re < 3 \times 10^5, \tag{3.3}$$

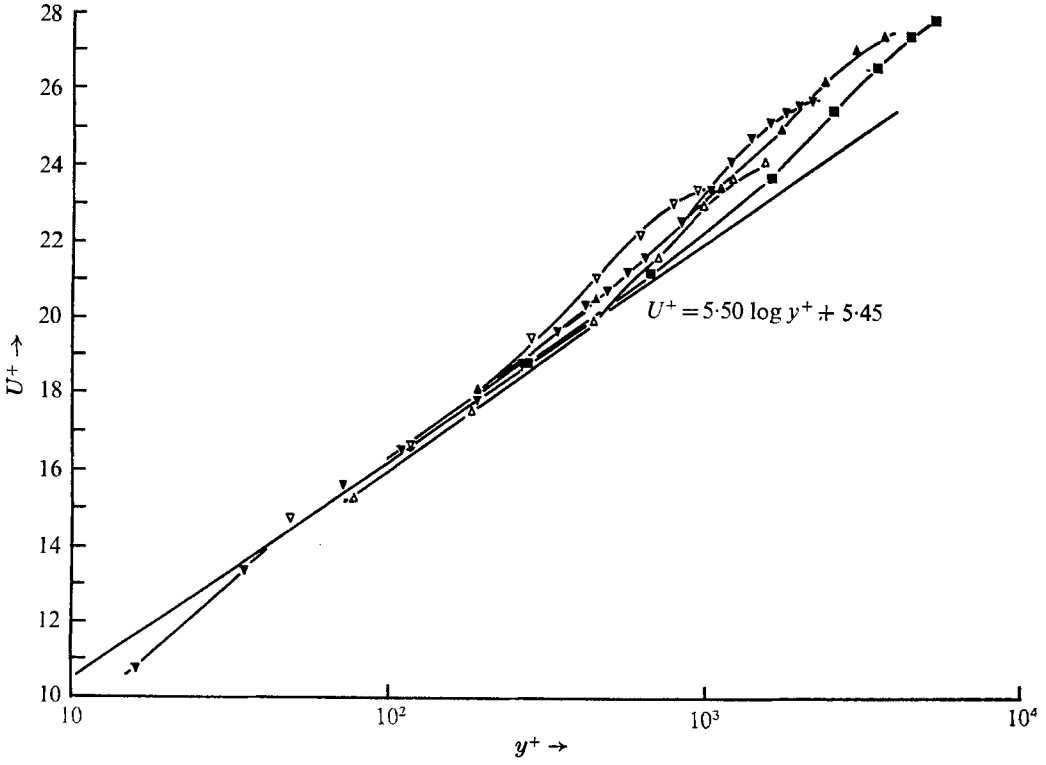

FIGURE 1. Non-dimensional velocity profiles.

Symbol	▽	△	▼	▲	■
Run	27	25	24	26	28
$Re \times 10^{-4}$	3·67	5·95	9·21	16·9	24·9

to within 3 %, and a U^+ versus y^+ plot (figure 1) shows a universal region obeying the Patel (1965) correlation

$$U^+ = 5{\cdot}50 \log y^+ + 5{\cdot}45. \tag{3.4}$$

The agreement with equation (3.4) is rather better than shown in figure 1, for the random error in friction velocity (estimated to be less than 3 %) may be partially eliminated by taking a smoothed friction factor curve in conjunction with the measured mass flow for each run. A velocity defect plot (figure 2) shows no systematic Reynolds number effect for $0 < r/a < 0{\cdot}9$, and the ratio of mean to maximum velocity, which is an indication of the degree of development of the flow, varied from 0·806 to 0·833 over the range $3{\cdot}5 \times 10^4 < Re < 2{\cdot}5 \times 10^5$. Nikuradse's (1932) ratios were somewhat larger than this (0·81 to 0·85) with $L/d = 120$, but so too were Laufer's with $L/d = 50$, so these results are inconclusive.

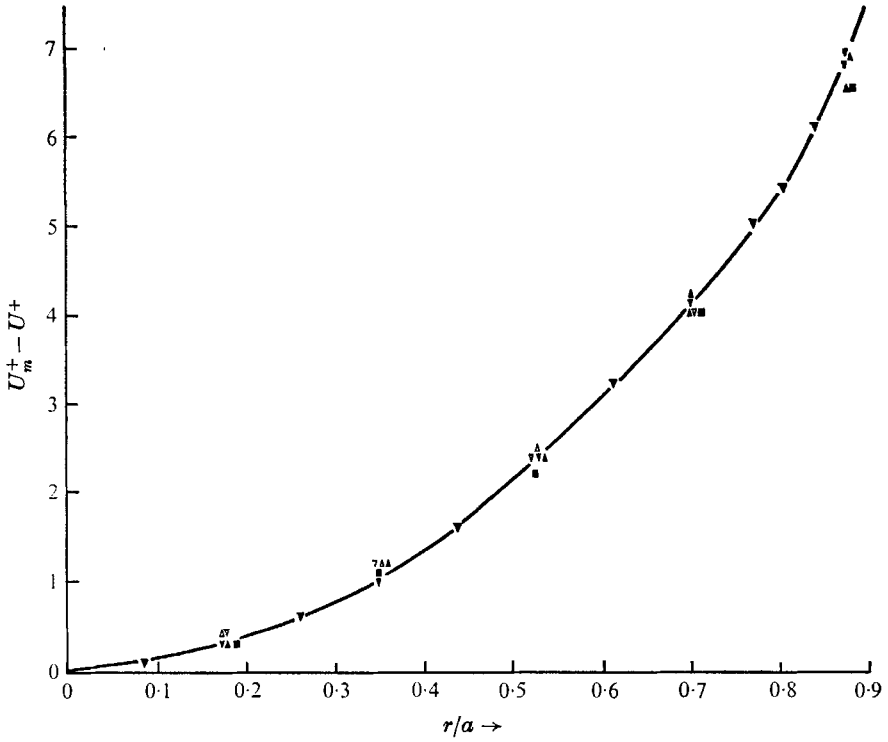

FIGURE 2. Velocity defect in a smooth pipe. Symbols same as figure 1.

The linearity of the measured turbulence shear stresses for four different Reynolds numbers (figure 3) does, however, encourage the belief that the flow was to all intents and purposes fully-developed. But although the distributions, taken in the same circumferential position, are linear in the range $r/a = 0 - 0{\cdot}8$ and give gradients of shear stress within 4 % of that anticipated from the pressure gradient results, the points on the $\overline{uv}/u_\tau^2$ plot are displaced an average distance of $0{\cdot}03a$ towards the pipe wall, contributing to errors of up to -9 % at $r/a = 0{\cdot}7$.

(For $r/a > 0{\cdot}8$, errors due to the large mean velocity variation along the wire are expected.) The small degree of asymmetry detected in the mean velocity profiles could perhaps be reflected in the shear stress distribution and some support for this is to be found in the absence of the discrepancy from earlier results taken in a different quadrant of the same duct (Lawn 1969).

The axial component of turbulence velocity, as measured by three different wire configurations at the same Reynolds number, is shown plotted in figure 4,

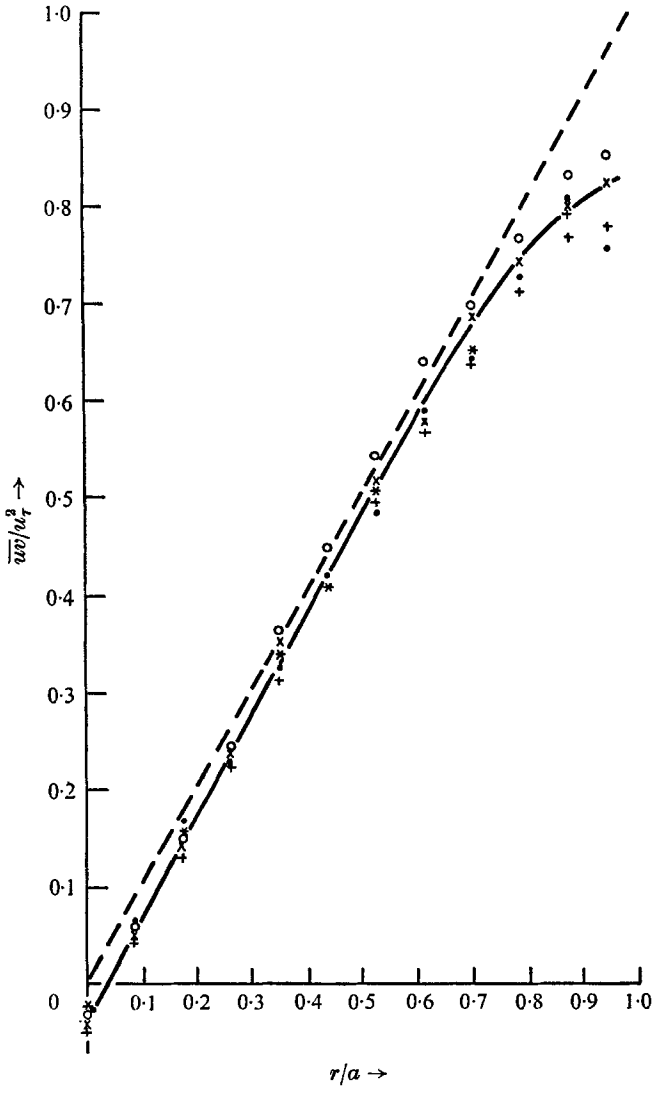

FIGURE 3. Shear stress measurements. ——, mean of measurements; - - -, deduced for symmetrical flow.

Symbol	●	×	+	○	*
Run	53	50	47	54	52
$Re \times 10^{-4}$	3·8	8·8–9·0		16·4	25·0

together with a somewhat arbitrarily drawn 'mean curve' from figure 5. Bands of $\pm 4\,\%$ about this curve embrace all the points for the four traverses. This is not, however, a measure of the standard deviation of a single point in a traverse, but of the run as a whole, for the deviations are largely systematic, indicating errors in calibration or friction velocity, or possibly of wire-response, rather than in recording.

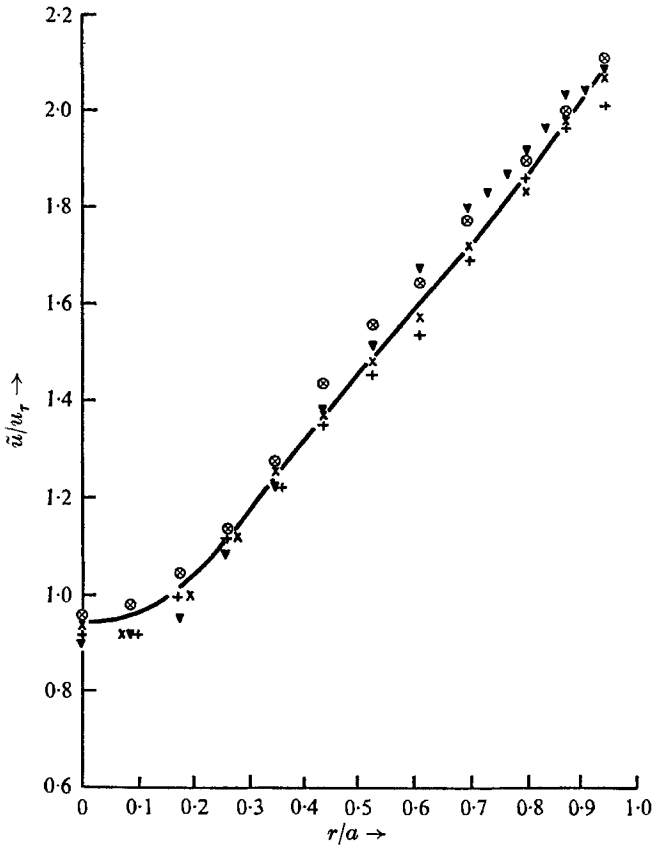

FIGURE 4. Fluctuating velocity distribution: one Reynolds number, $Re = 8{\cdot}7 - 9{\cdot}2 \times 10^4$. Run no.: ▼, 24 single-wire transverse; ⊗, 49, X-wire transverse; ×, 50, X-wire radial; +, 47, X-wire radial; ——, mean of measurements in figure 5.

This uncertainty of $\pm 4\,\%$ must be borne in mind when the results for four different Reynolds numbers are examined in figure 5. Thus although the low Reynolds number points ($Re = 3{\cdot}8 \times 10^4$) all lie below the mean line for $Re = 9{\cdot}0 \times 10^4$, and one set of high Reynolds number points ($Re = 16{\cdot}4 \times 10^4$) all lie on or above it, this trend cannot be considered significant, particularly as it is reversed by the highest Reynolds number ($Re = 25{\cdot}0 \times 10^4$). The same relationship between the runs is seen in the $\tilde{v}/u_\tau$ results, but again the differences are not statistically significant and this supports the contention above as to their origin. Of necessity the correlation coefficient is therefore also independent of Reynolds number (figure 5) and the similarity assumed in §2.1 is confirmed.

These results are similar to those of Laufer, except for the higher values of $\tilde{u}/u_\tau$ recorded near the centre-line of the duct in the present work. A Reynolds number of 9×10^4, intermediate between Laufer's, was selected for more detailed

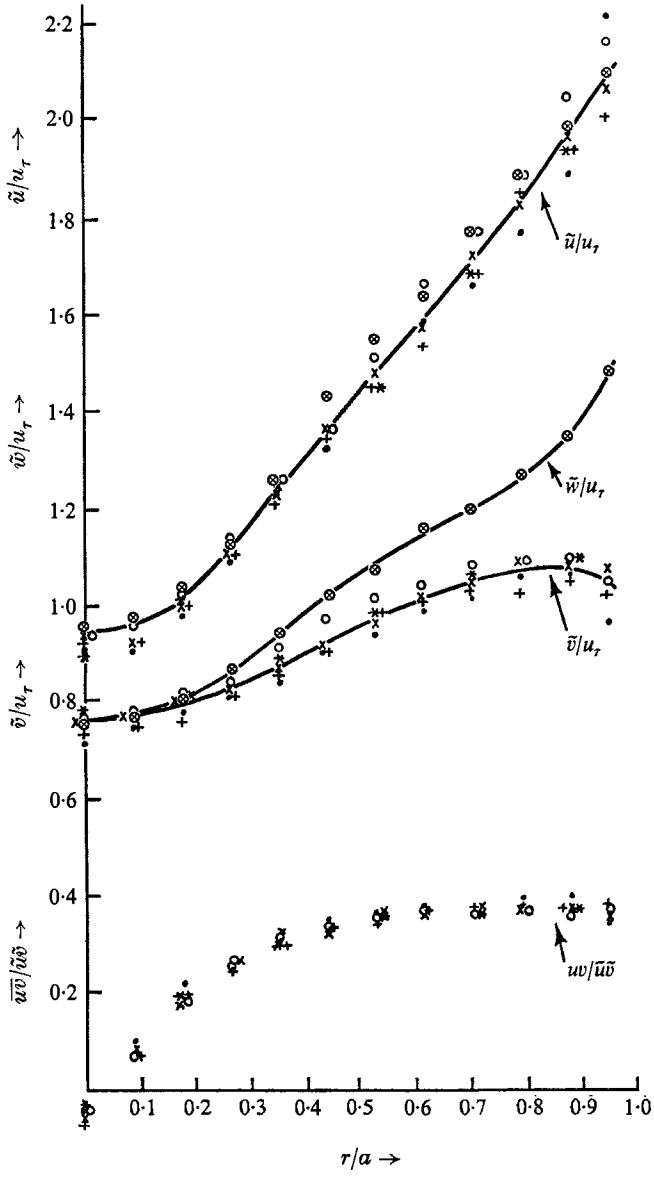

FIGURE 5. Fluctuating velocity distributions: several Reynolds numbers. ——, mean of measurements. X-wire measurements:

Symbols	●	⊗	×	+	○	*
Run	53	49	50	47	54	52
$Re \times 10^{-4}$	3·8	8·7 – 9·0			16·4	25·0

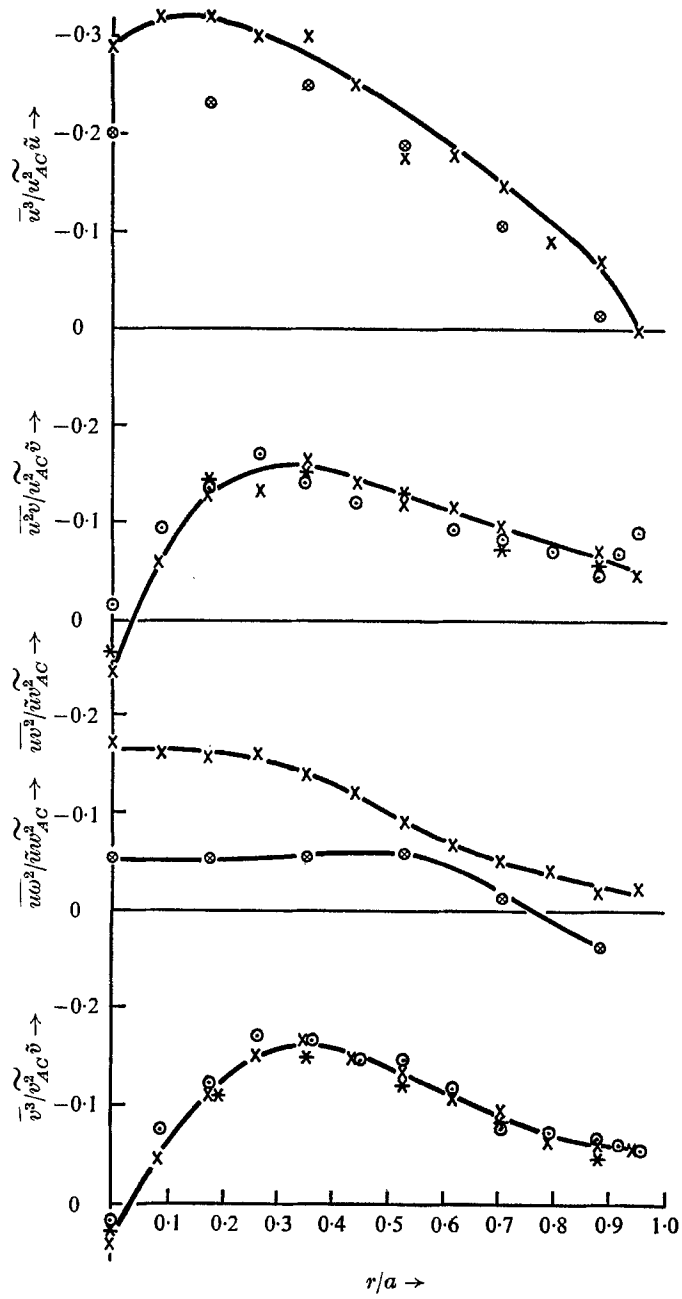

FIGURE 6. Triple correlation coefficients.

Symbol	⊗	×	⊙	*
Run	49	50	51	52
$Re \times 10^{-4}$	8·7 – 8·8		3·8	25·0

study as being a compromise between the inaccuracies in recording unsteady low-frequency signals and the poor response of the equipment to high frequency (see § 3.5).

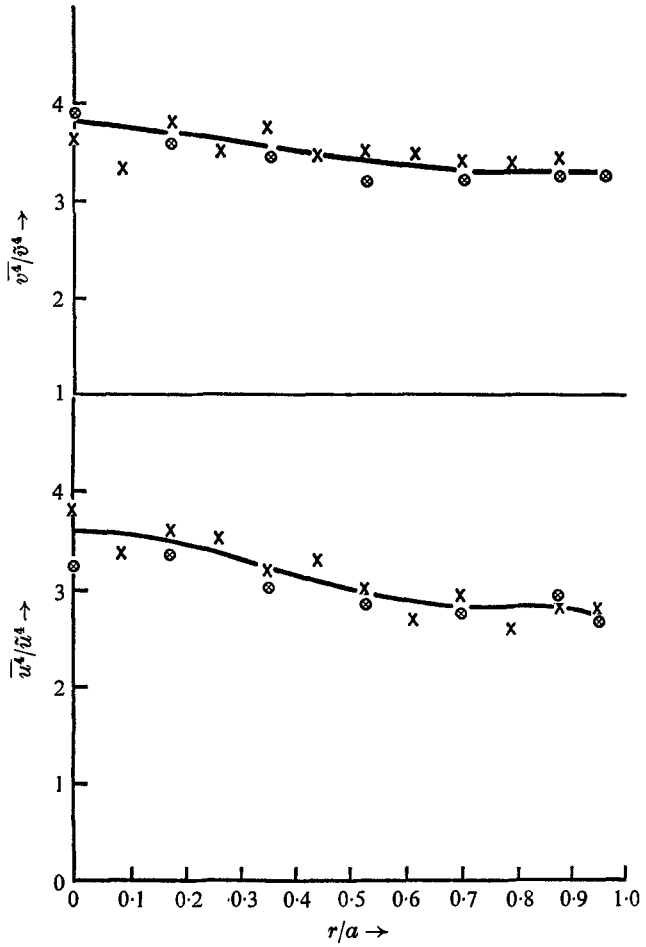

FIGURE 7. Flattening factors. $Re = 8{\cdot}8 - 9{\cdot}0 \times 10^4$: ⊗, run 48; ×, run 50.

3.3. *Multiple correlations*

The directly measured triple correlation coefficients appear in figure 6, and the flattening factor results in figure 7. These may be combined to give the true triple correlations through equations of the form

$$\frac{\overline{u^2v}}{\tilde{u}^2\tilde{v}} = \frac{\overline{u^2v}}{\widetilde{u^2_{AC}}\tilde{v}}\left[\frac{\overline{u^4}}{\overline{u^2}^2} - 1\right]^{\frac{1}{2}}, \tag{3.5}$$

where u^2_{AC} is the a.c. component of the squared velocity and the tilda superscript denotes r.m.s. values.

Once more there was a displacement in the apparent effective centre of the pipe, and once more there was no conclusive Reynolds number trend as far as the

'diffusion' results, $\overline{u^2v}/\widetilde{u^2_{AC}}\tilde{v}$ and $\overline{v^3}/\widetilde{v^2_{AC}}\tilde{v}$, were concerned. The skewness factor of u was measured with the wires first in the circumferential, and then in the radial plane, and a large discrepancy appears in the results, but both indicate no skewness at the point $r/a = 0{\cdot}9$. The correlations $\overline{uv^2}/\tilde{u}\widetilde{v^2_{AC}}$ and $\overline{uw^2}/\tilde{u}\widetilde{w^2_{AC}}$ were also measured, but $\overline{w^2v}/\widetilde{w^2_{AC}}\tilde{v}$ was not.

The two diffusion results agree qualitatively with Laufer's high Reynolds number values.

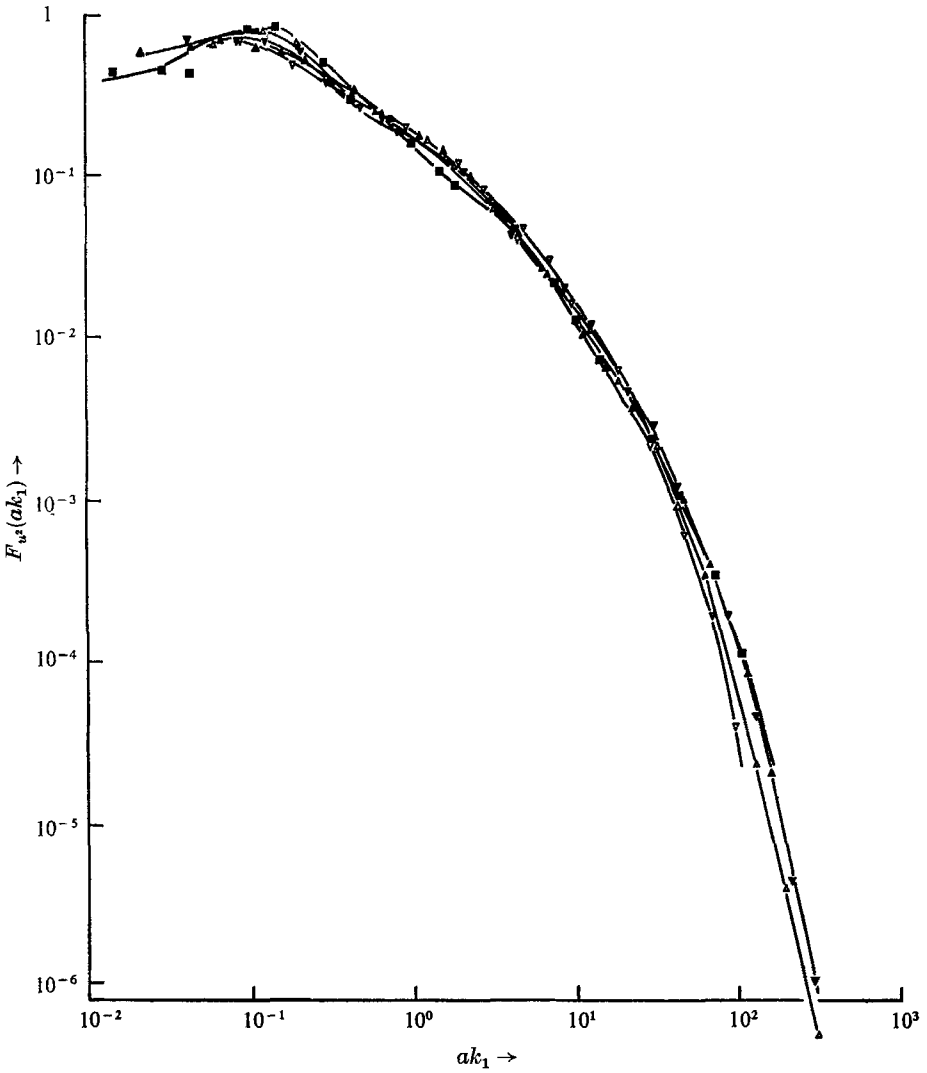

FIGURE 8. Power spectral density—axial component, wave-number plot. $r/a = 0{\cdot}35$. $Re \times 10^{-4}$: ∇, 3·67; △, 5·95; ▼, 9·21; ▲, 16·9; ■, 24·9.

3.4. *Spectral analysis*

The data was collected 'manually', by scanning through the frequency spectrum with a bandwidth of constant percentage (nominally 10 %). In the case of the power spectra, the upper frequency limit was determined by the limitations of

the anemometer: in the case of the cross-spectra, it was set at 2 kHz by the upper frequency limit of the modulator in the tape-recorder. The r.m.s. values of the filtered signals were normalized by the all-pass value, and the normalized spectral densities

$$F(n) = \left\{\frac{\tilde{\Delta}_{V(n)}}{V}\right\}^2 \frac{1}{\Delta_n}, \tag{3.6}$$

were integrated as a check on the technique. The average bandwidth of the analyser was thus deduced to be 12·8 % from a large number of integrations (one direct measurement at 175 Hz gave 12·5 %) and all the spectral density plots presented here, with two exceptions, then integrated to unity to within 6 % in the case of the axial velocity component and to within 10 % for the transverse velocity and shear stress spectra.

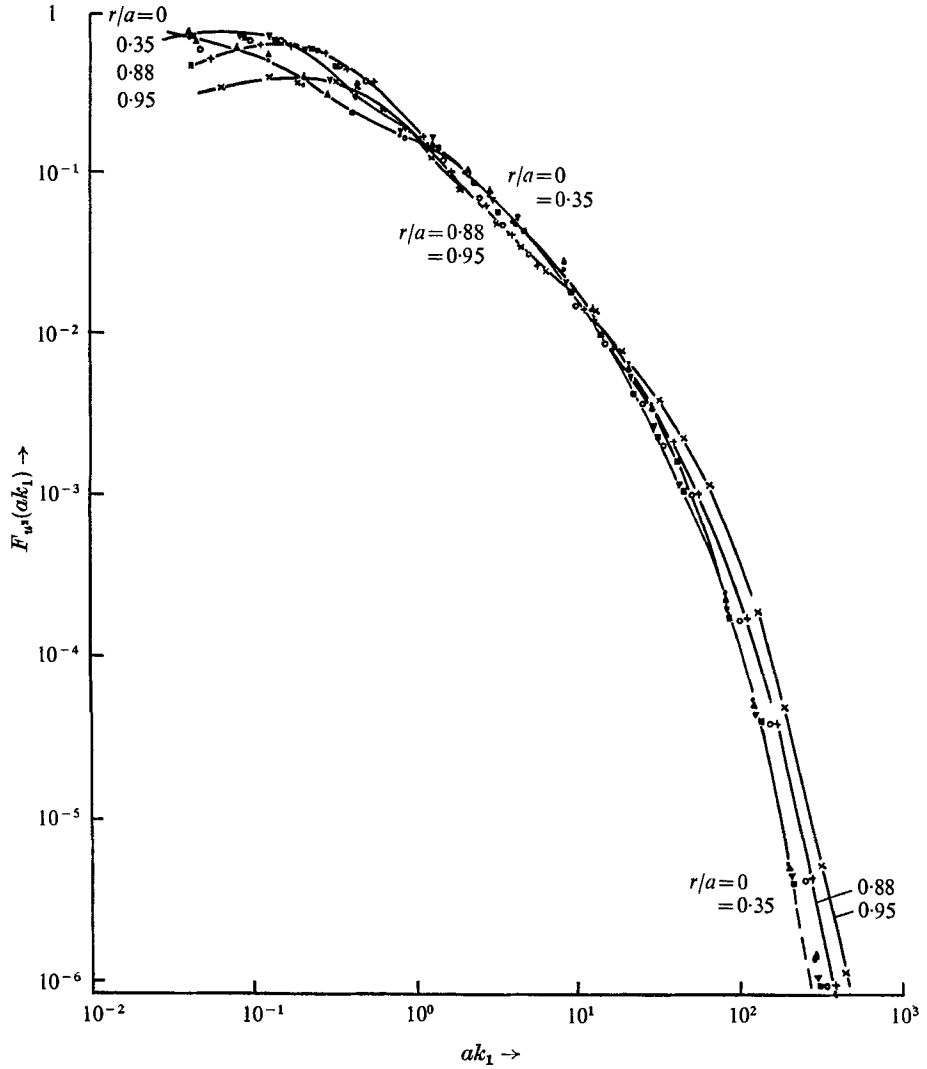

FIGURE 9. Power spectral density—axial component, single wire. $Re = 9 \times 10^4$. r/a: ●, 0·00; ▲, 0·18; ▼, 0·35; ■, 0·53; ○, 0·70; +, 0·88; ×, 0·95.

Conversion of the frequency plots to one-dimensional wave-number plots assuming Taylor's hypothesis was done in such a way as to maintain the normalization, i.e.

$$F(ak_1) = F(n)n/ak_1 = F(n)U/2\pi a. \tag{3.7}$$

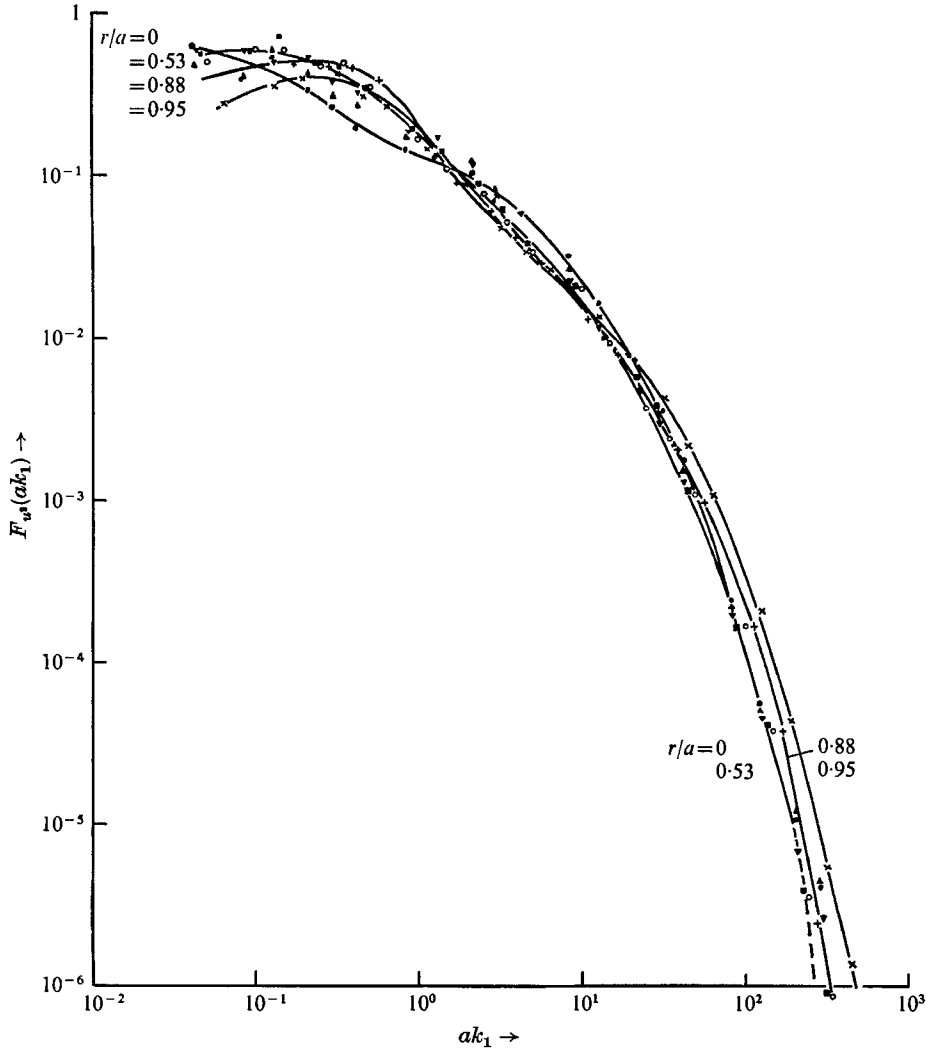

FIGURE 10. Power spectral density—axial component, X-wire. Values of r/a same as figure 9. $Re = 9 \times 10^4$.

The wave-number density functions obtained with a single wire at $r/a = 0{\cdot}35$ are plotted in figure 8 for a range of Reynolds numbers, and the influence of viscosity is clearly seen in the high wave-number dissipating motions. There does appear to be a 'saturation' effect at $Re = 10^5$, for the three highest Reynolds numbers have apparently identical high wave-number curves. This will be explained in § 3.5. Because only a very small fraction of the total energy is found in $ak_1 > 30$, the divergence of the curves in that region does not significantly

affect the low wave-number end, even though all curves must integrate to unity by definition.

Concentrating now upon the chosen Reynolds number, 9×10^4, the normalized power spectral density curves of the axial component for seven radial positions were obtained both with a single wire (figure 9) and with an X wire (figure 10). In positions of low turbulence intensity, there is evidence in both plots that noise in the electronic system obliterated the true signals at 7 kHz. However, comparison shows that the details of one plot are nearly all faithfully repeated in the second, encouraging confidence in the analysis technique and the addition of signals from two wires. Power spectral densities for the other components and the real component of the cross-spectral density are shown in figures 11 to 13. (The

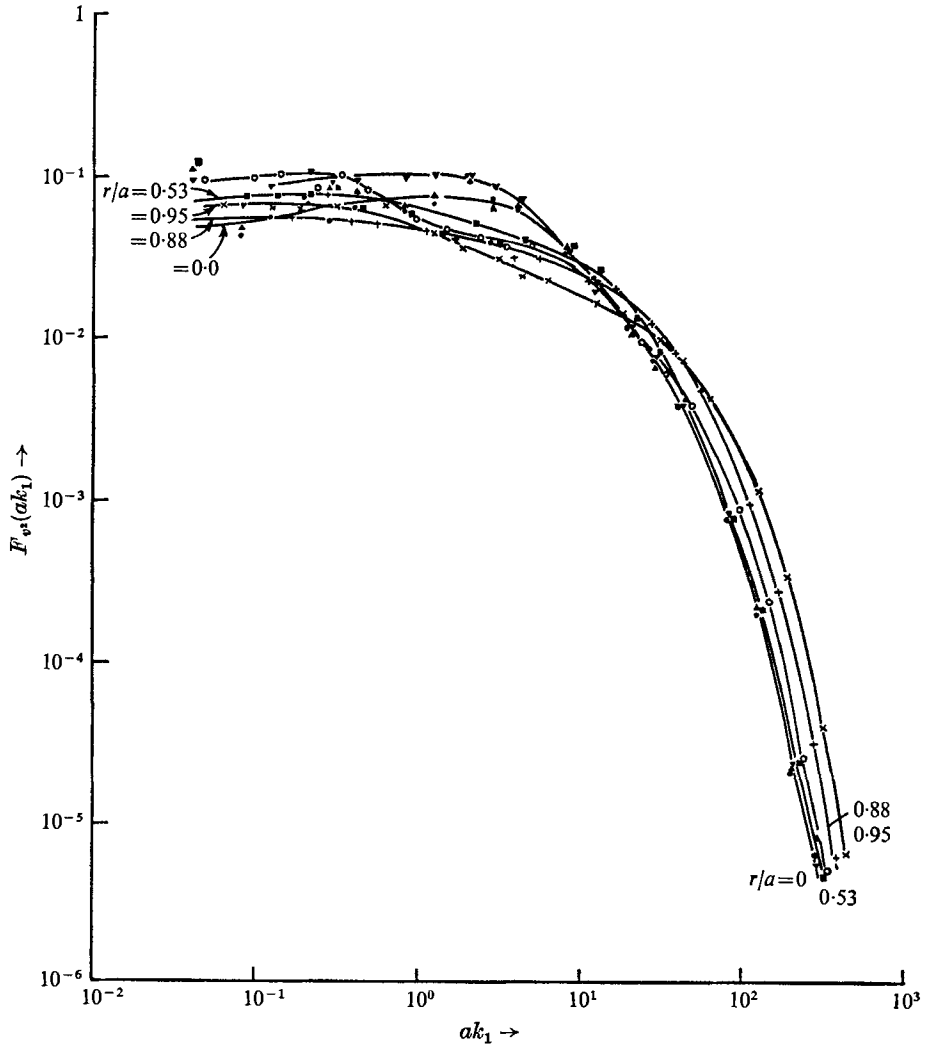

FIGURE 11. Power spectral density—radial component.
$Re = 9 \times 10^4$. Values of r/a same as figure 9.

two curves which do not integrate to unity to within 10 % are $F_{v^2}(ak_1)$ and $F_{w^2}(ak_1)$ at $r/a = 0{\cdot}35$.)

In order to compare the spectral distribution of energy between the components, the density functions $E_{u_iu_j}(ak_1)$ without normalization are plotted in figure 14 ($r/a = 0{\cdot}53$) and figure 15 ($r/a = 0{\cdot}88$). It emerges that the shear stress falls away far more rapidly than the energy at high wave-number, although it is still appreciable when the isotropic relation between E_{u^2} and E_{v^2}, equation (2.10),

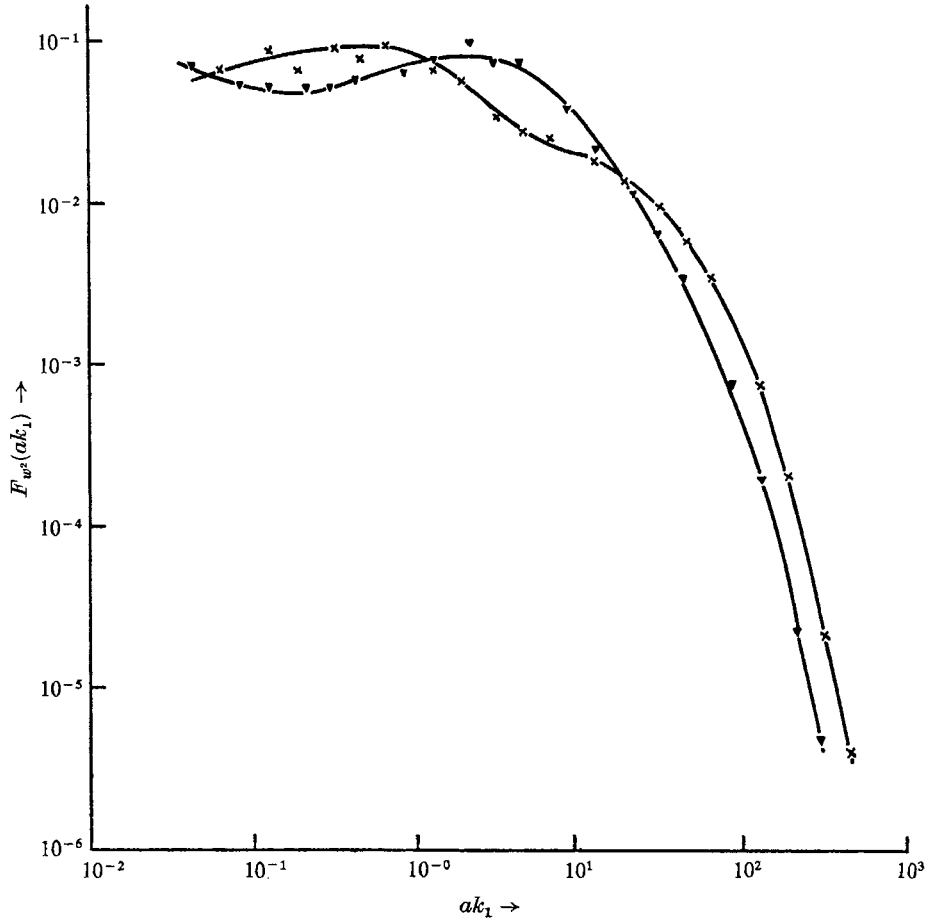

FIGURE 12. Power spectral density—circumferential component. $Re = 9 \times 10^4$. r/a: ▼, 0·35; ×, 0·95.

begins to hold approximately (to within 10 %). This is 'second-class local isotropy', and even before it is established, the power density functions begin to vary approximately as $k_1^{-\frac{5}{3}}$. (Only well away from the wall is there a clear range of wave-numbers with this variation.) As is seen in figure 16, the shear stress is so far from zero at this point ($ak_1 = 20$) that the correlation coefficient, $R_{uv}(ak_1)$ is as high as 0·4 for $r/a = 0{\cdot}88$.

3.5. *Deficiencies in hot-wire response*

No corrections have been applied to the data presented so far but two distinct types of error were certainly present.

The first has been discussed by Kovasznay (1954) and is the obvious one arising from the loss of response to high frequencies, inherent in the anemometer equipment. In fact, $ak_1 = 10^2$ corresponded to $n \sim 2{\cdot}5$ kHz at $Re = 9 \times 10^4$ on the pipe centre-line, but to $n \sim 7$ kHz at $Re = 2{\cdot}5 \times 10^5$, and since there was some loss of response above 3 kHz the higher Reynolds number results for $ak_1 > 10^2$ in figure 8, cannot possibly be correct. This partially accounts for the 'saturation' effect already noted. The same effect was almost certainly present in Laufer's results but no details of the frequency response of his system are given.

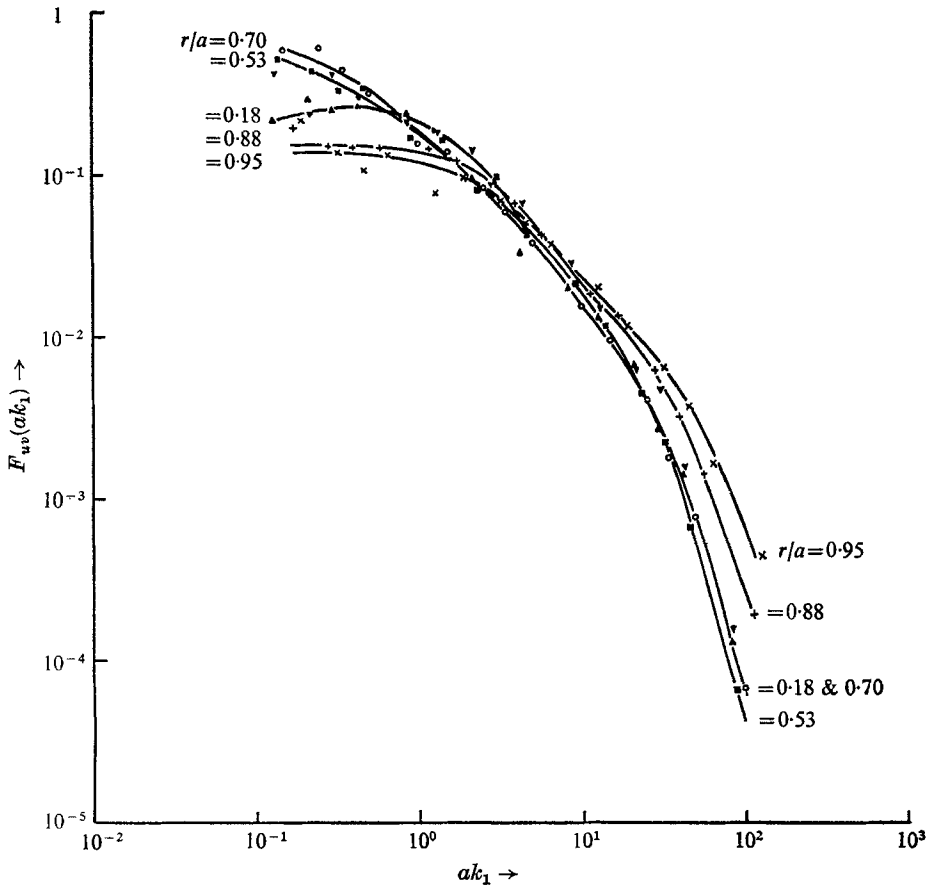

FIGURE 13. Cross spectral density—shear stress.
$Re = 9 \times 10^4$. Values of r/a same as figure 9.

The second type of error is due to the finite length of the wire and has been discussed by Uberoi & Kovasznay (1953), Frenkiel (1954) and Wyngaard (1968). (Laufer applied corrections to his measurements using the first paper.) Here we find from the second paper that the correction to turbulence velocities, including

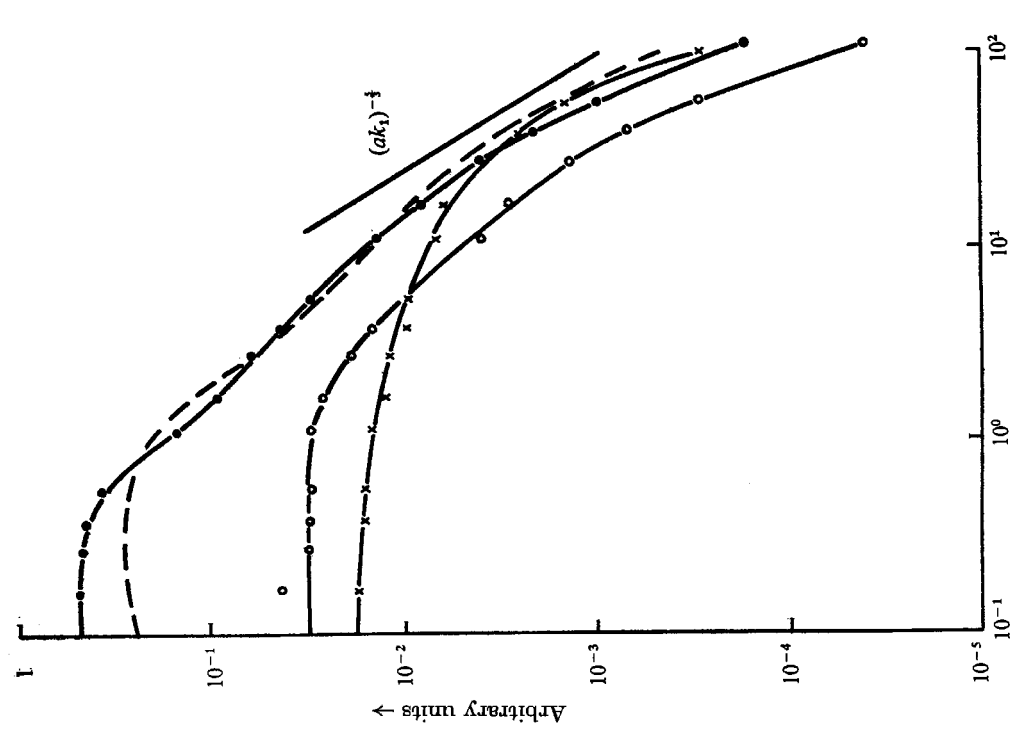

FIGURE 15. Spectral energy distribution between components. $r/a = 0{\cdot}88$; $\overline{u^2}/u_\tau^2 = 3{\cdot}96$; $\overline{v^2}/u_\tau^2 = 1{\cdot}09$; $\overline{uv}/u_\tau^2 = 0{\cdot}83$. $Re = 9 \times 10^4$. Symbols as in figure 14.

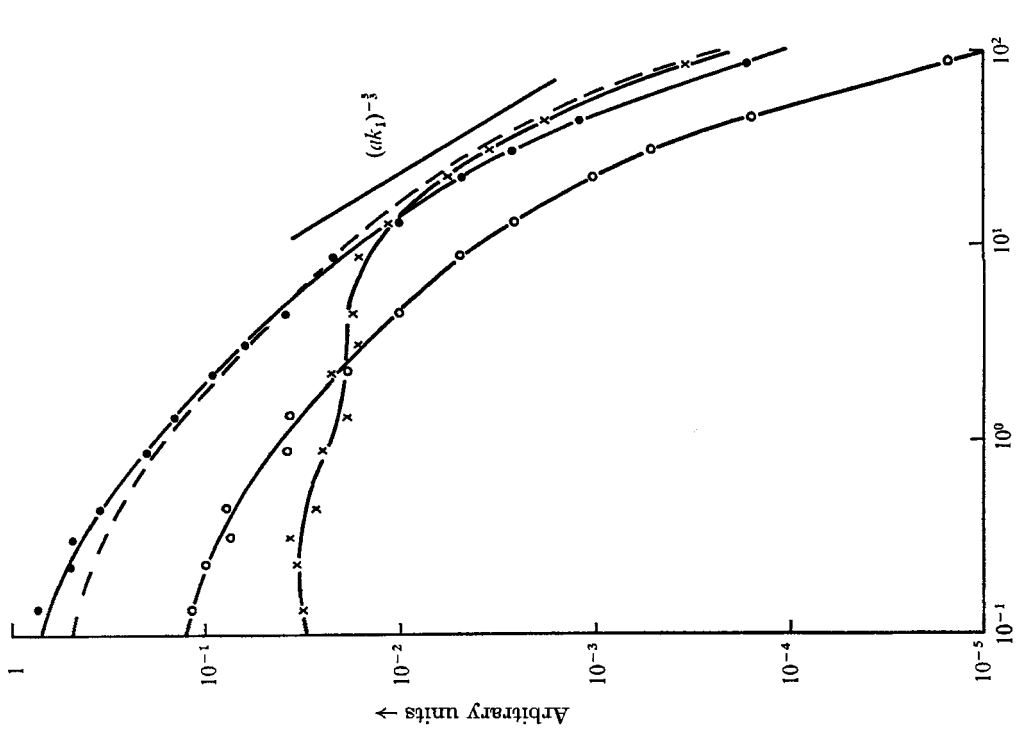

FIGURE 14. Spectral energy distribution between components. $r/a = 0{\cdot}53$; $\overline{u^2}/u_\tau^2 = 2{\cdot}22$; $\overline{v^2}/u_\tau^2 = 0{\cdot}97$; $\overline{uv}/u_\tau^2 = 0{\cdot}52$. $Re = 9 \times 10^4$. ●, $E_{us}(ak_1)$; ×, $E_{vs}(ak_1)$; ○, $E_{uv}(ak_1)$; - - -, $E_{vs}(ak_1)$ calculated from $E_{us}(ak_1)$ by isotropic relation.

all frequencies, is less than 2 % at $Re = 2{\cdot}5 \times 10^5$, but from the third paper, that the correction to the energy at non-dimensional wave-numbers, $ak_1 \sim 100$, may be as large as 20 % even at $Re = 9 \times 10^4$. Wyngaard evaluated the corrections for various ratios of Kolmogoroff length-scale to wire-length (here between 0·08 and 0·17 for $Re = 9 \times 10^4$), and also corrected for the effect of the lateral separation of the wires of an X probe. Note that the $k_1^{-\frac{5}{3}}$ regions of the spectra are not affected by these corrections at $Re = 9 \times 10^4$, but that deviations from the isotropic relation at slightly higher wave-numbers might be accounted for by the latter effect. At any rate, some correction is certainly necessary in evaluating the microscales, which depend on even higher wave-numbers.

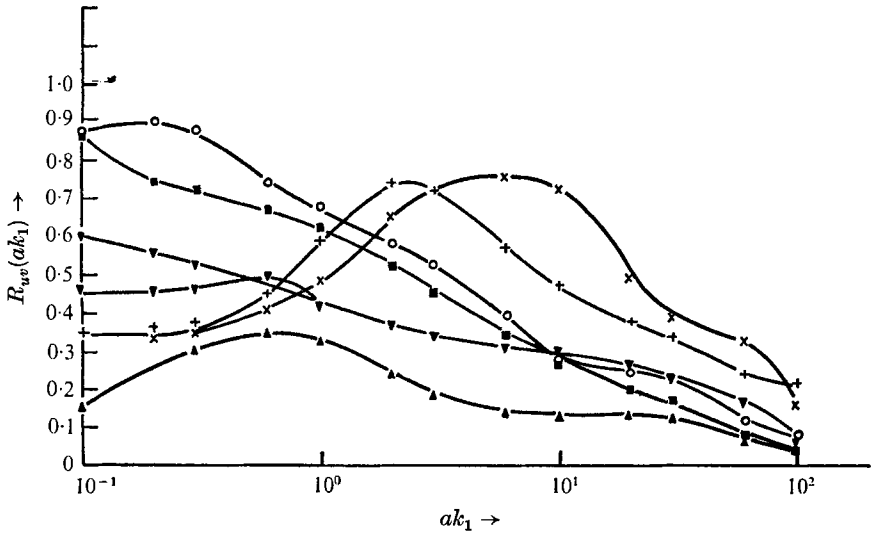

FIGURE 16. Local correlation coefficients in wave-number space.

$$R_{uv}(ak_1) = E_{uv}(ak_1)/[E_{u^2}(ak_1)E_{v^2}(ak_1)]^{\frac{1}{2}}.$$

r/a: ▲, 0·18; ▼, 0·35; ■, 0·53; ○, 0·70; +, 0·88; ×, 0·95.

3.6. *Microscales from the spectra*

By graphical integration of the spectral curves and use of

$$\frac{a^2}{\lambda_{xu}^2} = \int_0^\infty (ak_1)^2 F_{u^2}(ak_1)\, d(ak_1), \tag{3.8}$$

the variation of the microscales across the pipe radius was evaluated. Most of the results in figure 17 were obtained with an X probe having a wire separation of $\frac{1}{6}$ of the wire-length: these were not corrected. The correction to the single-wire results was, however, calculated from Wyngaard's published curves. It amounted to a reduction in λ_{xu}/a of 5 %, in the centre of the pipe, and of 16 % near the wall.

From the single-wire results was also calculated the variation of λ_{xu} with Reynolds number, represented in figure 18 by a^+. Now according to equation (2.4), $\lambda_{xu}/a \propto (a^+)^{-\frac{1}{2}}$, and this variation does approximately describe the measurements for the three lowest Reynolds numbers. Both types of error described above

prevented evaluation at the two highest Reynolds numbers. Taking the corrected value on the centre-line at $Re = 9 \times 10^4$, we have

$$\lambda_{xu}/a = 2{\cdot}8(a^+)^{-\frac{1}{2}}, \tag{3.9}$$

compared with Laufer's

$$\lambda_{xu}/a = 2{\cdot}3(a^+)^{-\frac{1}{2}} \tag{3.10}$$

based on $Re = 4{\cdot}3 \times 10^4$.

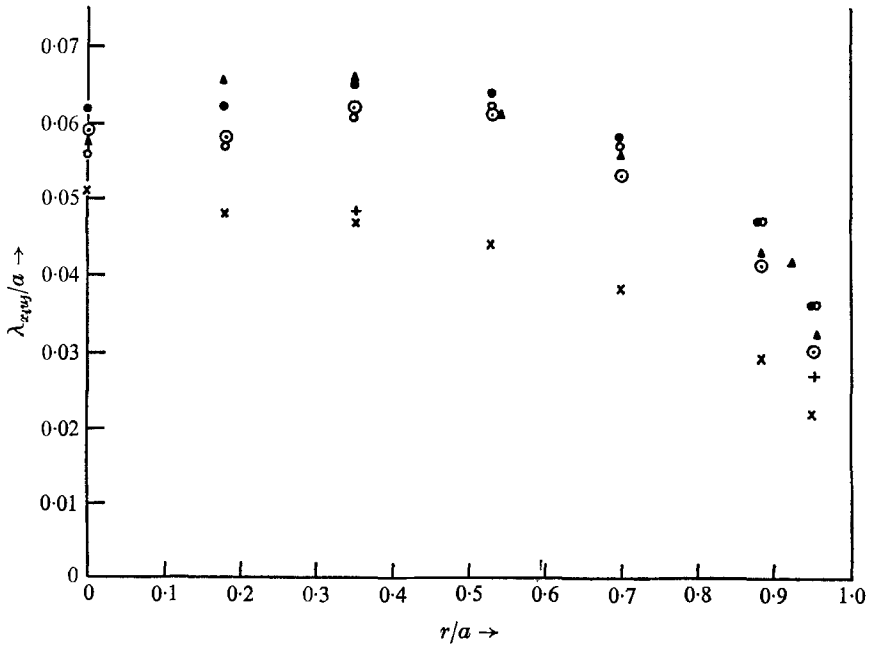

FIGURE 17. Radial distribution of microscales. $Re = 9 \times 10^4$.

	Spectra		Radial correlation	
λ_{xu}/a	●	single wire	λ_{ru}/a	▲
	⊙	single wire corrected		
	○	X-wire		
λ_{xv}/a	×	X-wire		
λ_{xw}/a	+	X-wire		

3.7. *Two-point correlations*

The two-wire probe, comprising parallel wires 1 mm long which could be moved to within 0·25 mm of each other, was used to measure the radial correlation coefficient, and the microscale was deduced from the relation for turbulence which is homogeneous on a small scale,

$$\frac{a^2}{\lambda_{ru}^2} = a^2\left[\frac{1-R_{u^2}(s)}{s^2}\right]_{s\to 0} \tag{3.11}$$

from plots such as figure 19. The fact that the points do not extrapolate to the

origin reduces confidence in the results, but only in two cases (for positions near the centre-line of the pipe) was the extrapolated correlation coefficient less than 0·97. Wire separations were determined by travelling microscope but because of a certain amount of bowing in both wires, the effective separation was not known to be better than 0·05 mm. More significant than this is the inaccuracy of the analogue correlator for signals with coefficients near unity and of low frequency (given as $\pm$ 0·03 by the manufacturers) and this probably accounts for the discrepancy from unity. It would result in a systematic error in $R_{u^2}(s)$ varying with the characteristic frequency of the signals but this should not affect the accuracy of the curvature measurements.

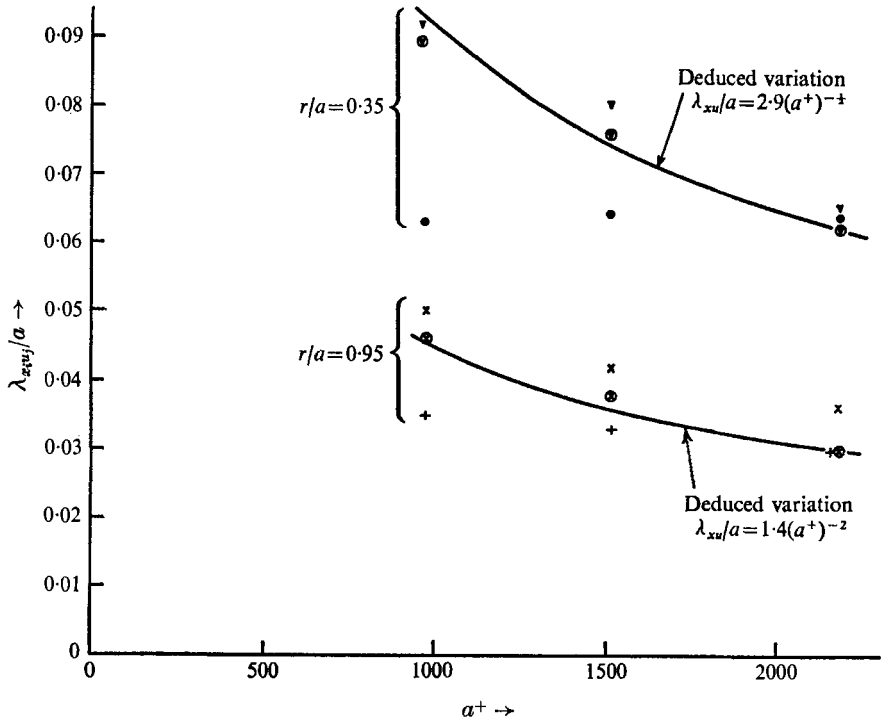

FIGURE 18. Reynolds number variation of microscales.

	Spectra	Radial correlation
r/a	λ_{xu}/a	λ_{ru}/a
0·35	▼ ⊖ corrected	●
0·95	× ⊗ corrected	+

The uncorrected results of these measurements are included in figures 17 and 18. At the selected Reynolds number, the microscales λ_{xu} and λ_{ru} agree closely over the whole of the radius, except quite close to the wall. However very little Reynolds number variation can be detected in λ_{ru}: either the results are in error or there is no structural similarity in the dissipating motions. This is further discussed in the following sections.

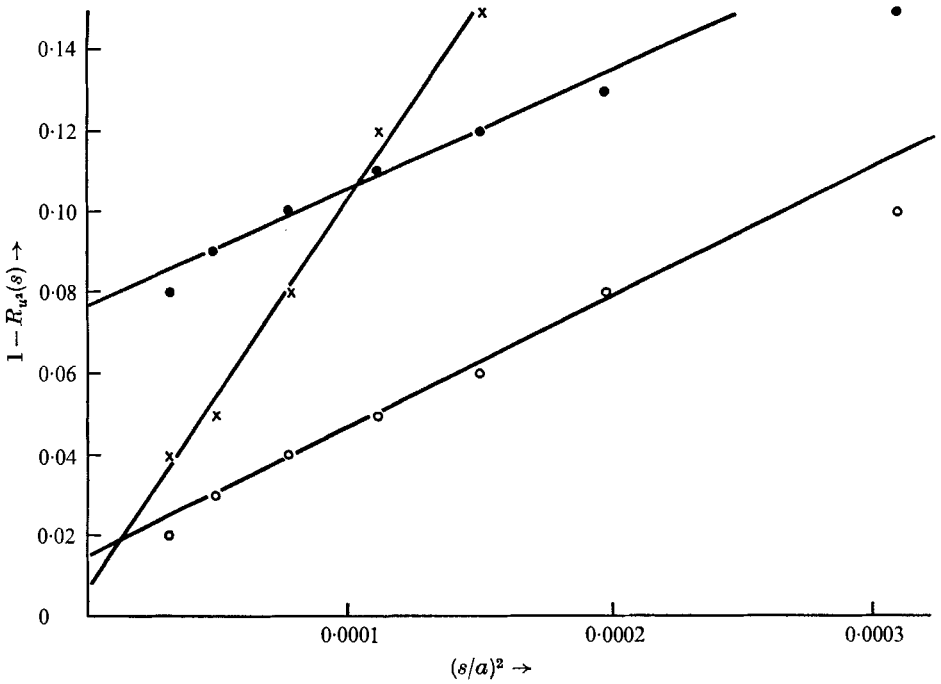

FIGURE 19. Determination of microscale from radial correlation measurements.
$Re = 9\times10^4$. $(a/\lambda_{ru})^2 = a^2[\{1-R_{u^2}(s)\}/s^2]_{s\rightarrow0}$.
r/a: ●, 0·0; ○, 0·70; ×, 0·95.

4. The rate of dissipation by classical methods

4.1. *Dissipation by difference*

The rate of dissipation may be estimated from equation (2.1) as the closing term in the balance with production and diffusion. The chief disadvantage of this approach is that the diffusion of pressure energy, as expressed by the $\overline{vp}/\rho$ correlation, has not been measured in duct flows, although Kobashi (1957) has made measurements in a wake. His results for the core of the flow show the pressure term having a magnitude one quarter of that of the kinetic energy diffusion, and the same variation. In this investigation, no measurements of the triple correlation $\overline{vw^2}$ were made either: from Laufer's results we expect

$$\overline{vw^2} \sim \tfrac{1}{2}\overline{v^3} \sim \tfrac{1}{2}\overline{u^2v}.$$

On this rather scanty evidence, an estimate for the total diffusion is

$$\frac{1}{r}\frac{d}{dr}\left\{r\left(\frac{\overline{vq^2}}{2}+\frac{\overline{vp}}{\rho}\right)\right\} \sim \frac{5}{4}\frac{1}{r}\frac{d}{dr}\left\{r\frac{\overline{vq^2}}{2}\right\} \sim \frac{5}{8}\frac{1}{r}\frac{d}{dr}\{r\tfrac{5}{4}(\overline{v^3}+\overline{u^2v})\}$$

$$\sim \frac{3}{4}\frac{1}{r}\frac{d}{dr}\{r(\overline{u^2v}+\overline{v^3})\} \qquad (4.1)$$

but this could be considerably in error. It is, however, likely to be a more reasonable estimate than one based upon the complete neglect of pressure diffusion.

The diffusion was evaluated using (4.1) from the graphical differentiation of the triple correlation results for $Re = 9 \times 10^4$. The distribution is shown in figure 20. Because the triple products could not be measured right up to the wall, it is not possible to check the divergence calculation by integration of the diffusion curve. Clearly, however, the wall layer loses energy rapidly to the core, as was observed by Laufer.

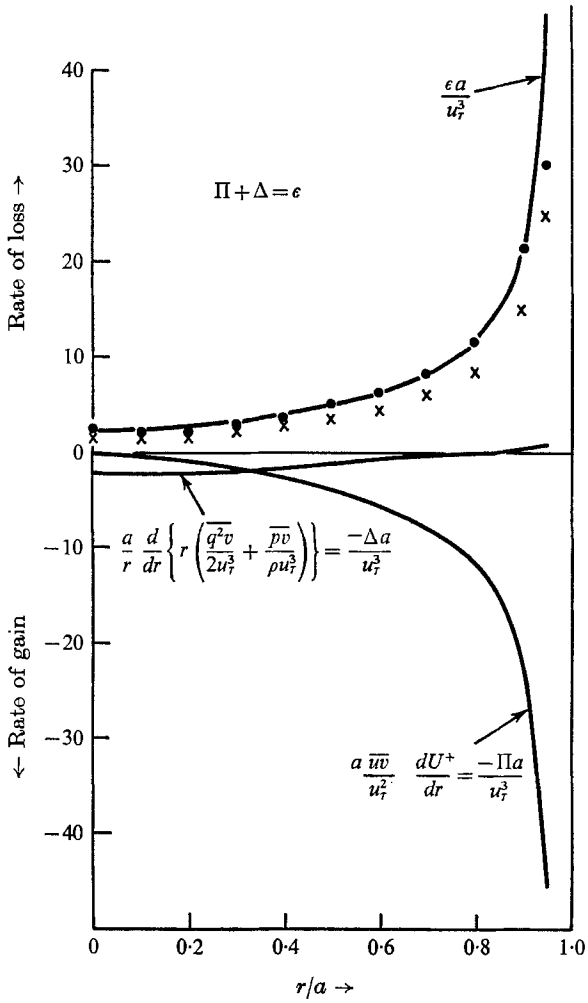

FIGURE 20. Turbulence energy balance. Dissipation determined: ——, by difference; ×, from microscales; ●, from Kolmogoroff hypothesis.

The rate of strain of the mean flow was determined by graphical differentiation of the velocity defect plot to give the rate of production of turbulence energy. Relatively little error may be expected in this procedure.

Addition of the rates of production and diffusion leads to the dissipation curve in figure 20. Once more there is close similarity with Laufer's low Re results, but here the presence of an equilibrium layer (in which production and dissipation

are locally balanced) between $r/a = 0{\cdot}7$ and $0{\cdot}9$, is more clearly indicated, because Laufer's measured diffusion rate was still appreciable in this layer, whereas in the present work it was negligible.

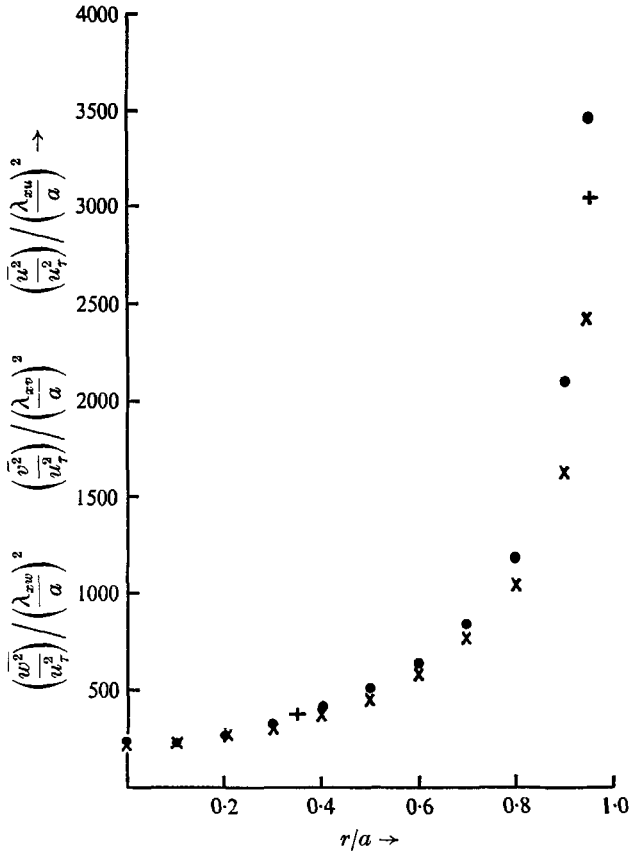

FIGURE 21. Comparison of velocity derivatives. $Re = 9 \times 10^4$.

$$\bullet,\ \left(\frac{\bar{u}^2}{u_\tau^2}\right)\Big/\left(\frac{\lambda_{xu}}{a}\right)^2 = \overline{\left(\frac{\partial u}{\partial x}\right)^2}\left(\frac{a^2}{u_\tau^2}\right);\quad \times,\ \left(\frac{\bar{v}^2}{u_\tau^2}\right)\Big/\left(\frac{\lambda_{xv}}{a}\right)^2 = \frac{1}{2}\overline{\left(\frac{\partial v}{\partial x}\right)^2}\left(\frac{a^2}{u_\tau^2}\right);$$
$$+,\ \left(\frac{\bar{w}^2}{u_\tau^2}\right)\Big/\left(\frac{\lambda_{xw}}{a}\right)^2 = \frac{1}{2}\overline{\left(\frac{\partial w}{\partial x}\right)^2}\left(\frac{a^2}{u_\tau^2}\right).$$

4.2. *Degree of isotropy*

Of the four velocity derivatives measured, two, $\overline{(\partial u/\partial x)^2}$ and $\frac{1}{2}\overline{(\partial u/\partial r)^2}$, have already been effectively compared, for in figure 17, the equality of λ_{xu} and λ_{ru} (for $r/a < 0.8$) implies equality of these derivatives as demanded by isotropy. Two more, $\frac{1}{2}\overline{(\partial v/\partial x)^2}$ and $\frac{1}{2}\overline{(\partial w/\partial x)^2}$, computed from the uncorrected spectra, are compared with $\overline{(\partial u/\partial x)^2}$ in figure 21, and again the isotropic demand for equality is met in the range $r/a < 0{\cdot}8$.

As the maximum contributions to the integral of the form (3.8) come from non-dimensional wave-numbers $ak_1 \sim 10^2$, the evidence of figure 16 is also in

favour of a high degree of isotropy in the dissipating motions, for $r/a < 0{\cdot}8$ at any rate ($R_{uv}(ak_1) < 0{\cdot}1$).

These remarks apply to $Re = 9 \times 10^4$, but from figure 18 it appears that they do not apply to smaller Reynolds numbers. It may well be that at smaller Reynolds numbers, the production and dissipation ranges of the spectrum are not sufficiently separated for complete isotropy, and this is in agreement with Laufer's results for $Re = 4{\cdot}0 \times 10^4$.

4.3. *Dissipation from the microscales*

The microscale results for $Re = 9 \times 10^4$ suggest that equation (2.5), which assumes complete isotropy, will not be grossly in error. However, dissipation estimated from this equation is compared with that estimated by difference in figure 20, and is seen to be systematically in error by -29 % (with a random scatter of only 3 %) in the range $r/a < 0{\cdot}9$. This compares with Laufer's -50 % systematic error for $Re = 4{\cdot}3 \times 10^5$, using only some of the isotropic relations between derivatives (see §2.2).

Rather than reject the possibility of isotropy at the higher Reynolds numbers, we may attribute these discrepancies to poor high-frequency response, and in particular, to finite wire-length, the errors increasing with Reynolds number. Thus it is suggested that Laufer's low Reynolds number results ($Re = 4{\cdot}0 \times 10^4$) are indeed correct (and they do agree with the present ones, obtained 'by difference') and that the dissipating motions are still far from isotropic. Isotropy is approached as the Reynolds number increases and is already a good approximation at $Re = 9 \times 10^4$, but by then errors in hot-wire response begin to disrupt the measurements if the ratio of wire-length to pipe radius is greater than 10^{-2}, as it was here. From the corrections calculated for single wires in §3.6, the necessary correction to the dissipation calculated from X-wire data at $Re = 9 \times 10^4$ is seen to be at least 10 % in the centre and 35 % near the wall, which largely accounts for the observed discrepancy in the present work.

5. The rate of dissipation assuming an inertial subrange

Taking a value of 0·55 for K in equation (1.7), the dissipation rate was estimated from the smoothed spectral curves of figure 10 for $Re = 9 \times 10^4$, by fitting tangents of slope $-\frac{5}{3}$ by eye. The best fit was at $ak_1 = 15$ for spectra from the centre of the pipe, rising to $ak_1 = 30$ near the wall. The values of dissipation shown in figure 20 were thus derived, and in the range $0 < r/a < 0{\cdot}9$, they deviate from the curve calculated by difference by less than 15 %.

Use of the inner law for K of 0·51, proposed by Bradshaw (1967*a*), would also put the $r/a = 0{\cdot}95$ value within 15 % of the curve. However, in the core region, a value of $K = 0{\cdot}53$ is indicated from the present work and this leads to a standard deviation of only 8 % from the smoothed results obtained by difference. The uncertainty in the latter results in the centre of the pipe, where diffusion predominates, is probably also of this order, but the agreement between the two methods is not appreciably worse here than in the equilibrium region near the wall, for which there is considerable confidence in the deduced value of ϵ. (This

confidence is, it must be admitted, based upon the assumption of negligible pressure diffusion.)

It was stated in §2.3 that the condition (1.6) for the existence of an inertial subrange may be translated to $Re_\lambda \gtrsim 140$ for pipe flow. In the present work, the range of Re_λ was $115 < Re_\lambda < 200$. Moreover, the apparently least accurate value of ϵ was near the pipe wall where Re_λ was lowest, so the condition appears to be the correct one, implying that $Re > 10^5$ for an inertial subrange in the whole of the core-flow. This confirms the conclusions concerning isotropy in §§4.2 and 4.3 and (1.6) may also be taken as the condition for the dissipating motions to be isotropic.

The advantage of the method of measuring ϵ afforded by assuming equation (1.7) has been pointed out by Bradshaw: the spectrum need only be accurately measured at moderate frequencies, instead of at ones an order of magnitude greater. Unfortunately the assumption of Taylor's hypothesis remains implicit in the method, but a good estimate of dissipation in any duct or boundary-layer flow should be obtained by using it, provided the Reynolds number is high enough.

6. Conclusion

Turbulence energy measurements in the core region of turbulent pipe flow strongly suggest that the dissipating motions are effectively isotropic for $Re \gtrsim 10^5$ and that the hypothesis of second-class isotropy provides the best way of measuring the dissipation rate, by assuming an inertial subrange even in the presence of shear. The formula

$$E_{u^2}(k_1) = 0{\cdot}53\epsilon^{\frac{2}{3}}k_1^{-\frac{5}{3}} \tag{6.1}$$

gives an estimate of the dissipation rate ϵ with a standard deviation of 8 % for $Re = 9 \times 10^4$ and $0 < r/a < 0{\cdot}9$. This is in good agreement with the data of Bradshaw (1967*a*, *b*) for other shear flows.

Although the 'direct' measurements of dissipation rate by Laufer (1954) and the present author at 'high' Reynolds numbers were probably in error, due to the inadequacy of the hot-wire system, these measurements are to be preferred for $Re < 10^5$, when local isotropy is a poor approximation.

This paper is published by permission of the Central Electricity Generating Board.

REFERENCES

Batchelor, G. K. 1956 *The Theory of Homogeneous Turbulence.* Cambridge University Press.

Bradshaw, P. 1967*a* *NPL Aero Rep.* 1220.

Bradshaw, P. 1967*b* *Aero. Res. Counc. R. & M* 3603.

Comte-Bellot, G. 1965 *Publ. Sci. et Tech. du Ministere de l'Air*, no. 419.

Frenkiel, F. N. 1954 *Roy. Aero. Soc. Quart.* **5**, 1.

Hinze, J. O. 1959 *Turbulence.* McGraw Hill.

Klebanoff, P. S. 1955 *NACA Rep.* 1247.

Kobashi, Y. 1957 *J. Phys. Soc. Japan*, **12**, 533.

KOLMOGOROFF, A. N. 1941 *C.R. Acad. Sci. U.S.S.R.*, **30**, 301.
KOVASZNAY, L. G. 1954 *NACA TR* 1209.
LAUFER, J. 1954 *NACA Rep.* 1174.
LAWN, C. J. 1969 *CEGB*/RD/B/M1277.
LAWN, C. J. 1970 *CEGB*/RD/B/N1575A, B and C.
NIKURADSE, J. 1932 *VDI Forschungsheft*, 356.
PATEL, V. C. 1965 *J. Fluid Mech.* **23**, 185.
STEWART, R. W. & TOWNSEND, A. A. 1951 *Phil. Trans. Roy. Soc.* A **243**, 359.
UBEROI, M. S. & KOVASZNAY, L. S. G. 1953 *Quart. Appl. Math.* **10**, 375.
WYNGAARD, J. C. 1968 *J. Sci. Instr.* series 2, **1**, 1105.